

## EFFICIENT COMPUTATION, SENSITIVITY, AND ERROR ANALYSIS OF COMMITTOR PROBABILITIES FOR COMPLEX DYNAMICAL PROCESSES\*

JAN-HENDRIK PRINZ<sup>†</sup>, MARTIN HELD<sup>‡</sup>, JEREMY C. SMITH<sup>§</sup>, AND FRANK NOÉ<sup>¶</sup>

**Abstract.** In many fields of physics, chemistry, and biology, the characterization of rates and pathways between certain states or species is of fundamental interest. The central mathematical object in such situations is the committor probability—a generalized reaction coordinate that measures the progress of the process as the probability of proceeding to the target state rather than relapsing to the source state. Here, we conduct a numerical analysis of the committor. First, it is shown that committors can be expressed by the stationary eigenfunctions of a modified dynamical operator, thus relating the committors to the dominant eigenfunctions of the original operator. Based on this reformulation, committors can be efficiently computed for systems with large state spaces. Moreover, a sensitivity analysis of the committor is conducted, which allows its statistical uncertainty from estimation to be quantified within a Bayesian framework. The methods are illustrated on two examples of diffusive dynamics: a two-dimensional model potential with three minima, and a three-dimensional model representing protein-ligand binding.

**Key words.** Markov state model, diffusion dynamics, committor probability, uncertainty estimation, Bayesian inference, error analysis

**AMS subject classifications.** 60J22

**DOI.** 10.1137/100789191

**1. Introduction.** The essential features of dynamical systems can often be understood in terms of the transitions between substates of special interest. This is particularly true where the dynamics are metastable, thus defining a natural partition into long-living substates. Examples of this include protein folding or misfolding [21,24], molecular association [29], chemical reactions [8], phase transitions in spin systems [13, 23, 25] or liquids [30], climate systems [11], and trend changes in financial systems [10]. In many cases, characterizing the dynamics between two substates  $\mathcal{A}, \mathcal{B}$  of configurational space  $\Omega$  provides a satisfactory picture of the process (e.g., in protein folding  $\mathcal{A}$  being unfolded and  $\mathcal{B}$  native [21]), whereas in other cases the simultaneous consideration of multiple substates is necessary.

It is now widely recognized that the committor probability, also called splitting probability or probability of folding in some contexts, is the central mathematical

---

\*Received by the editors March 18, 2010; accepted for publication (in revised form) January 4, 2011; published electronically DATE.

<http://www.siam.org/journals/mms/x-x/78919.html>

<sup>†</sup>IWR, University of Heidelberg, Im Neuenheimer Feld 368, 69120 Heidelberg, Germany. Current address: DFG Research Center Matheon, FU Berlin, Arnimallee 6, 14195 Berlin, Germany (prinz@mi.fu-berlin.de). This author acknowledges funding from the DFG International Graduate College 710 and also funding from the DFG Research Center Matheon.

<sup>‡</sup>Institute for Mathematics and Computer Science, FU Berlin, Arnimallee 6, 14195 Berlin, Germany (martin.held@fu-berlin.de). This author acknowledges funding from the DFG.

<sup>§</sup>UT/ORNL Center for Molecular Biophysics, Oak Ridge National Laboratory, P.O.Box 2008, Oak Ridge, TN 37831-6164 (smithjc@ornl.gov). This author acknowledges support from grant initiative DE-PS02-08ER08-13 “Multiscale Mathematics and Optimization for Complex Systems” from the Offices of Biological and Environmental Research and Advanced Scientific Computing of the United States Department of Energy.

<sup>¶</sup>DFG Research Center Matheon, FU Berlin, Arnimallee 6, 14195 Berlin, Germany (frank.noe@fu-berlin.de). This author acknowledges funding from DFG grant 825/1-2 and also funding from the DFG Research Center Matheon.

object needed for intersubstate processes to be characterized [2, 3, 5, 6, 7, 12, 14, 15]. The committor  $q(x)$  is a state function that provides the probability at any state  $x \in \Omega$  of next moving to  $\mathcal{B}$  rather than to  $\mathcal{A}$  under the action of the system dynamics. By definition,  $q(x) = 0$  for  $x \in \mathcal{A}$  and  $q(x) = 1$  for  $x \in \mathcal{B}$ .<sup>1</sup> The committor thus defines a dynamical reaction coordinate, which has the advantage over ad hoc reaction coordinates that it does not bring the danger of concealing relevant dynamics of the system. In the present work, we investigate how the committor probability can be efficiently computed for large-scale systems and study its sensitivity as well as its uncertainty in cases where the full dynamics have been inferred from a finite set of observations.

We concentrate here on dynamical systems which can be modeled as Markov processes between a finite (but possibly large) number  $m$  of discrete states. This includes systems which are discrete and Markovian by definition, such as spin glasses and on-lattice Go models [32] or resulting from a space discretization of a continuous generator or propagator [26]. In the latter case, the spatial discretization will cause the discretized system to be no longer exactly Markovian. The unintentionally introduced memory can in principle be described by the Mori–Zwanzig formalism when projecting the full-dimensional dynamics onto a basis set defining the discrete states [18, 36, 37], but, from a numerical point of view the error made by using a Markov model in the discrete-state space can in principle be rendered as small as desired by using a fine enough discretization, a small enough time resolution [26], or, alternatively, embedding the dynamics in an extended discrete state space as proposed in [31].

The system dynamics are then described by a time-discrete transition matrix  $T(\tau) \in \mathbb{R}^{m \times m}$ , giving rise to the Chapman–Kolmogorov equation

$$(1) \quad \mathbf{p}(k\tau) = \mathbf{p}(0)\mathbf{T}^k(\tau),$$

which propagates state probabilities  $p \in \mathbb{R}^m$  in time, or by the rate matrix  $\mathbf{K} \in \mathbb{R}^{m \times m}$  and the corresponding master equation

$$\frac{d\mathbf{p}(t)}{dt} = \mathbf{p}(t)\mathbf{K}$$

with the formal solution

$$(2) \quad \mathbf{p}(t) = \mathbf{p}(0) \exp(t\mathbf{K}),$$

yielding the formal relationship

$$\mathbf{T}(\tau) = \exp(\tau\mathbf{K}).$$

Numerous studies treat the estimation of  $\mathbf{T}$  or  $\mathbf{K}$  from observation data in cases where they are not defined by the model itself or can be derived from the discretization of a continuous operator [4, 12, 16, 35], but this estimation problem is not further considered here.

Given such a dynamical model, let us examine a number of aspects of the system dynamics that can be accessed *via* the committor probability. First all sets of constant committor probability in the state space  $\Omega$ ,

$$(3) \quad I(q^*) = \{x \in \Omega \mid q(x) = q^*\} \quad \forall q^* \in [0, 1],$$

---

<sup>1</sup>An alternative definition in time-discrete dynamics is to check also for  $x \in \mathcal{A} \cup \mathcal{B}$ , where  $x$  is in the next timestep. In this case  $q(x \in \mathcal{A}) \neq 0$  and  $q(x \in \mathcal{B}) \neq 1$  can occur. For time-continuous systems, both definitions are equal.

are hypersurfaces that partition the state space into the two disjoint subsets  $I_{\mathcal{A}}(q^*) = \{x \in \Omega \mid q(x) < q^*\}$  with  $\mathcal{A} \subset I_{\mathcal{A}}(q^*) \forall q^* > 0$  and  $I_{\mathcal{B}}(q^*) = \{x \in \Omega \mid q(x) > q^*\}$  with  $\mathcal{B} \subset I_{\mathcal{B}}(q^*) \forall q^* < 1$ . The committor is thus a measure for the progress of a process or reaction; i.e., it is the ideal reaction coordinate for the process  $\mathcal{A} \rightarrow \mathcal{B}$  [2, 7, 14]. Of special interest in this context is the isocommittor surface  $I(0.5)$ , which can be interpreted as the transition state ensemble in protein folding theory [24].

Once the committor has been computed, the change of any state variable  $a(x)$  along the  $\mathcal{A} \rightarrow \mathcal{B}$  process may be monitored by projecting onto this reaction coordinate using

$$(4) \quad a(q^*) = \mathbb{E}(a(x) \mid x \in I(q^*)) = \frac{\int_{x \in I(q^*)} dx \pi(x) a(x)}{\int_{x \in I(q^*)} dx \pi(x)}$$

with  $\pi(x)$  proportional to the statistical weight of state  $x$  and also the stationary distribution of state  $x$ , if this exists. In the latter case, one can define a dimensionless potential of mean force along the  $\mathcal{A} \rightarrow \mathcal{B}$  process given by

$$(5) \quad F(q^*) = - \log \frac{\int_{x \in I(q^*)} dx \pi(x)}{\int_{x \in \Omega} dx \pi(x)}.$$

The transport properties from  $\mathcal{A}$  to  $\mathcal{B}$  can be computed *via* transition path theory (TPT) [17, 33]. In particular, the reactive flux  $f_{ij}$  between two states  $i$  and  $j$  is given by

$$(6) \quad f_{ij} = \pi_i q_i^- k_{ij} q_j^+$$

for rate matrices [17], or

$$(7) \quad f_{ij}(\tau) = \pi_i q_i^- T_{ij}(\tau) q_j^+$$

if the transition probability matrix is used [21]. Here,  $q^-$  is the backward committor, which is the probability that of the two states set  $\mathcal{A}$  has been visited last and not  $\mathcal{B}$  which is equal to  $1 - q^+$  if the dynamics are reversible. The reactive flux  $f_{ij}$  is proportional to the probability that a reactive trajectory, that is, a trajectory directly connecting  $\mathcal{A}$  and  $\mathcal{B}$ , passes through the transition  $i \rightarrow j$ . The net transport through  $i \rightarrow j$  is given by

$$(8) \quad f_{ij}^+ = \max\{f_{ij} - f_{ji}, 0\},$$

which defines a network flow out of  $\mathcal{A}$  and into  $\mathcal{B}$  that can be decomposed into a set of  $\mathcal{A} \rightarrow \mathcal{B}$  reaction pathways along with their probabilities [17, 21, 33].

Finally, one can also express different rates using the committor probability. The *global*  $\mathcal{A} \rightleftharpoons \mathcal{B}$  flux  $F$  from TPT, which is defined as the average number of trajectories traveling between  $\mathcal{A}$  and  $\mathcal{B}$  per time unit, is given by [17]

$$(9) \quad F = \sum_{i \in \mathcal{A}, j \notin \mathcal{A}} f_{ij} = \sum_{i \in \mathcal{A}, j \notin \mathcal{A}} f_{ij}^+.$$

$F$  is the inverse expected time needed for an  $\mathcal{A} \rightleftharpoons \mathcal{B}$  cycle, composed of the inverse forward rate constant  $k_{\mathcal{A}\mathcal{B}}$  and the inverse backward rate constant  $k_{\mathcal{B}\mathcal{A}}$ :

$$(10) \quad F^{-1} = k_{\mathcal{A}\mathcal{B}}^{-1} + k_{\mathcal{B}\mathcal{A}}^{-1}.$$

In order to calculate these rate constants we need the *milestoning* probability  $\pi_{\mathcal{A}}^{mile}$ , which is the total probability that the process has been in  $\mathcal{A}$  previously while  $\pi_{\mathcal{B}}^{mile} = 1 - \pi_{\mathcal{A}}^{mile}$  is the probability that it has been in  $\mathcal{B}$  previously:

$$(11) \quad \pi_{\mathcal{A}}^{mile} := \sum_{j \in \Omega} \pi_j q_j^-.$$

We have the following detailed balance condition:

$$(12) \quad \pi_{\mathcal{A}}^{mile} k_{\mathcal{A}\mathcal{B}} = (1 - \pi_{\mathcal{A}\mathcal{B}}^{mile}) k_{\mathcal{B}\mathcal{A}},$$

and we derive the expression for the  $\mathcal{A} \rightarrow \mathcal{B}$  rate constant as

$$(13) \quad k_{\mathcal{A}\mathcal{B}} = (\pi_{\mathcal{A}}^{mile})^{-1} F.$$

For alternative rate definitions and their relations, see, e.g., [34].

Given the fundamental relevance of the committor probability in the characterization of dynamical processes, it is important to be able to compute  $q(x)$  efficiently, and also to understand its sensitivity to perturbations, especially in cases where the system dynamics can be computed only approximately, e.g., by some sampling scheme such as molecular dynamics simulations or Monte–Carlo dynamics. The remainder of the paper will concentrate on these numerical questions together with the illustration of the methods process on a simple two-dimensional (2D) energy surface with metastable states and on a three-dimensional (3D) model reminiscent of protein–ligand association.

**2. Committor equations.** The committor is defined as the probability of reaching state  $\mathcal{B}$  before state  $\mathcal{A}$  is visited and thus corresponds to the result of a hypothetical experiment which starts an infinite number of Monte–Carlo simulations in state  $s$  and measures  $\mathbf{q}_s$  as the fraction of simulations, that reach  $\mathcal{B}$  first.

**2.1. Transition matrix.** We first derive the committor equations *via* the hitting times  $h^{\mathcal{A}}(x)$  of a subset  $\mathcal{A} \subset \Omega$ , which corresponds to the minimal number of steps a stochastic process needs to reach the set  $\mathcal{A}$ . Let  $h^{\mathcal{A}}(X)$  be the hitting time to reach set  $\mathcal{A}$  given by

$$h^{\mathcal{A}}(X) = \inf \{n : X_n \in \mathcal{A}, n \in \mathbb{N}^+\}$$

with  $X_i : i \rightarrow \Omega$  a time-discrete stochastic process.

Now consider the committor probability,  $q_i^+$  pertaining to two sets  $\mathcal{A}$  and  $\mathcal{B}$ , which is the probability that, starting in state  $i$ , the system goes to  $\mathcal{B}$  next rather than to  $\mathcal{A}$  using the hitting times  $h$ :

$$q_i^+ \equiv \mathbb{P}_i(h^{\mathcal{B}} < h^{\mathcal{A}}),$$

where  $\mathbb{P}_i$  indicates the probability for all trajectories  $X$  that originate in state  $i$ .

In order to compute  $q_i^+$ , we use the recursive relation in the committor between connected points in configurational space  $\Omega$ , which states that the committor probability of a state  $i \notin \mathcal{A} \cup \mathcal{B}$  is given by the sum of all products of the probabilities of reaching a neighboring state  $j$  given from the transition probability  $T_{ij}$  and the committor probability at state  $j$ , while for states  $\mathcal{A}$  and  $\mathcal{B}$  we set the given solution to be in correspondence with the boundary conditions:

$$(14) \quad q_i^+ = \begin{cases} 0 & \text{if } i \in \mathcal{A}, \\ 1 & \text{if } i \in \mathcal{B}, \\ \sum_j T_{ij} q_j^+ & \text{if } i \notin \mathcal{A}, \mathcal{B}. \end{cases}$$

The backward committor probability  $q_i^-$  is defined, respectively, as the probability that being in state  $i$ , the system was in  $\mathcal{B}$  last rather than in  $\mathcal{A}$ . In order to obtain the backward committor, we use the backward propagator

$$T_{ij}^- := \frac{\pi_j}{\pi_i} T_{ji},$$

which contains the probabilities that if the system is in state  $i$ , then it came from state  $j$ . Proceeding in analogy to the forward committor, we get

$$q_i^- = \begin{cases} 1 & \text{if } i \in \mathcal{A}, \\ 0 & \text{if } i \in \mathcal{B}, \\ \sum_{j \in I} T_{ij}^- q_j^- & \text{if } i \notin \mathcal{A}, \mathcal{B} \end{cases}$$

for the backward committor. For reversible dynamics the forward and backward propagators are equal,  $T_{ij} = \frac{\pi_j}{\pi_i} T_{ji} = T_{ij}^-$ , from which it follows immediately that

$$q_i^- = 1 - q_i^+.$$

**2.2. Rate matrix.** Given the rate matrix  $K \in \mathbb{R}^{m \times m}$ , we can use a similar argument as for the time-discrete case and derive expressions for the committor:

$$\begin{aligned} q_i^+ &= 0 & \text{if } i \in A, \\ q_i^+ &= 1 & \text{if } i \in B, \\ \sum_{j \in I} K_{ij} q_j^+ &= 0 & \text{if } i \notin A \cup B. \end{aligned}$$

The corresponding equations hold also for the backward committor. A proof can be found in [17, 22].

**2.3. Transforming between rate and transition matrices.** It turns out that there is a simple way to transform rate matrices into transition matrices, and vice versa, that leaves the committor probabilities unchanged. This transformation is useful when a method is available to compute the committor from the transition matrices, but not for rate matrices, or vice versa.

**THEOREM 1.** *Let  $\mathbf{T}(\mathbf{K}) \in \mathbb{R}^{m \times m}$  be a stochastic matrix and  $\mathbf{K} \in \mathbb{R}^{m \times m}$  be a rate matrix related by the transformation*

$$(15) \quad \mathbf{T}(\mathbf{K}) = \frac{c}{c_{max}} \mathbf{K} + Id, \quad 0 < c < 1$$

with  $c_{max} = -\min_{i \in \{1, \dots, m\}} K_{ii}$  representing the largest entry in the rate matrix. Then  $\mathbf{T}(\mathbf{K})$  and  $\mathbf{K}$  have the same committor probabilities for any choice of  $\mathcal{A}, \mathcal{B} \subset \Omega$ .

See the appendix for the proof. The theorem allows for the methods explained later to be used with equal computational effort for rate matrices. In particular, it can transport a potential sparse structure of the rate matrix to a transition matrix and thus allows for sparse eigensystem algorithms in these cases as well.

**2.4. Numerical solution.** The committor equations (14) can be solved with any linear systems solver. When the system is very large and sparse, a sparse linear systems solver may still be able to handle them efficiently. An alternative approach to computing the committor probability from  $\mathbf{K}$  has been proposed in [13]. However, this approach requires the  $\mathbf{K}$ -matrix to be inverted, which effectively limits its applicability to systems of  $\leq 10^4$  states.

**3. Eigenvector formulation.** An alternative view is obtained when formulating the committor problem in terms of the dominant eigenvectors of either  $\mathbf{K}$  or  $\mathbf{T}(\tau)$ . This is useful from a numerical point of view, because efficient solvers, such as the Power method or Krylov subspace methods, exist for dominant eigenvectors. Moreover, it is useful from a physical standpoint as it allows the committor to be understood in terms of the slowest relaxation process of the system.

An approach to approximate  $\mathbf{q}(x)$  in terms of the second eigenvector of  $\mathbf{K}$  or  $\mathbf{T}(\tau)$  has been proposed in [1]. This approach is valid only if the second eigenvector is similar to the  $\mathcal{A} \rightarrow \mathcal{B}$  committor and the second and third eigenvalues are well separated. In molecular processes, this is often referred to as “two-state” process, where there exists one slow process that is clearly separated from all other processes in terms of timescales. In the following, we will derive equations that allow the committors to be computed exactly in terms of their dominant eigenvectors for any Markovian system.

**3.1.  $\mathcal{A} \rightarrow \mathcal{B}$  committor.** We construct a transition matrix  $\hat{\mathbf{T}}$  with absorbing states  $\mathcal{A}$  and  $\mathcal{B}$  from  $\mathbf{T}$  by

$$(16) \quad \hat{T}_{ij} = \begin{cases} T_{ij}, & i \notin \mathcal{A} \cup \mathcal{B}, \quad j \in X, \\ 1, & i \in \mathcal{A} \cup \mathcal{B}, \quad j = i, \\ 0, & i \in \mathcal{A} \cup \mathcal{B}, \quad j \neq i, \end{cases}$$

assuming that the underlying dynamics is ergodic or equivalently  $\mathbf{T}$  irreducible. We then define a transition matrix  $\hat{\mathbf{T}}^\infty$  that transports any initial distribution infinitely into the future,

$$(17) \quad \hat{\mathbf{T}}^\infty = \lim_{n \rightarrow \infty} \hat{T}^n,$$

and consequently directly into either state  $\mathcal{A}$  or  $\mathcal{B}$ . Then the committor  $q_s$  of state  $s$  is given by the total sum of probabilities after propagating a distribution located only in  $s$  given by a canonical unit vector  $(\mathbf{e}^s)_i = \delta_{is}$  into the future using  $\hat{\mathbf{T}}$ :

$$(18) \quad q_s = \sum_{k \in \mathcal{B}} ((\mathbf{e}^s)^T \hat{\mathbf{T}}^\infty)_k = \sum_{k \in \mathcal{B}} \hat{T}_{sk}^\infty.$$

In the following we will show that  $\mathbf{T}^\infty$  and thus  $\mathbf{q}$  can be computed quickly and robustly.

Without loss of generality, we treat here the case where the sets  $\mathcal{A} = \{a\}$  and  $\mathcal{B} = \{b\}$  consist of only one state each. In cases where the sets are larger, they can simply be aggregated into a single state in the definition of  $\hat{\mathbf{T}}$ . Finally the matrix is diagonalized, obtaining

$$(19) \quad \hat{\mathbf{T}}^\infty = \mathbf{R} \cdot \lim_{n \rightarrow \infty} \text{diag}(\lambda_1^n, \lambda_2^n, \dots, \lambda_N^n) \cdot \mathbf{R}^{-1}$$

with  $\mathbf{R} := [\mathbf{r}_1, \dots, \mathbf{r}_N]$  being the matrix of right eigenvectors of  $\hat{\mathbf{T}}$ , and  $\lambda_i$  are the corresponding eigenvalues, sorted from the largest to the smallest modulus of the eigenvalue. It follows from the Perron–Frobenius theorem that there exist exactly two left<sup>2</sup> eigenvectors with eigenvalue 1,  $\mathbf{e}^a$  and  $\mathbf{e}^b$ . The modulus of all other eigenvalues is strictly smaller than 1. As a result,

$$(20) \quad \lim_{n \rightarrow \infty} |\lambda_i^n| = 0 \quad \forall \lambda_i < 1,$$

---

<sup>2</sup>The number of left and right eigenvectors to the same eigenvalue are equal.

and thus

$$(21) \quad \hat{\mathbf{T}}^\infty = \mathbf{R} \cdot \text{diag}(1, 1, 0, \dots, 0) \cdot \mathbf{R}^{-1}.$$

We now define  $\mathbf{L} := \mathbf{R}^{-1}$  to be the inverse of the eigenvector matrix.  $\mathbf{L}$  is a matrix of left eigenvectors, since all of its rows fulfill the requirement for a left eigenvector with the same diagonalized eigenvalue matrix

$$(22) \quad \mathbf{L} \cdot \hat{\mathbf{T}}^\infty = \mathbf{L} \Lambda.$$

This means that once we have the basis of left eigenvectors that equal  $\mathbf{R}^{-1}$  we can avoid the expensive calculation of the inverse. Although this is no advantage in general, in the present case the left eigenvectors of  $\hat{\mathbf{T}}^\infty$  take a particularly simple form. We choose the following representation by row vectors for  $\mathbf{L} := [\mathbf{l}_1, \dots, \mathbf{l}_N]^T$  and get

$$(23) \quad \hat{\mathbf{T}}^\infty = [\mathbf{r}_1, \dots, \mathbf{r}_N] \cdot \text{diag}(1, 1, 0, \dots, 0) \cdot [\mathbf{l}_1, \dots, \mathbf{l}_N]^T$$

$$(24) \quad = [\mathbf{r}_1, \mathbf{r}_2] \cdot [\mathbf{l}_1, \mathbf{l}_2]^T.$$

As mentioned before, the left eigenvectors to the eigenvalue of 1 are a linear combination of  $\mathbf{e}^a$  and  $\mathbf{e}^b$ :

$$(25) \quad [\mathbf{l}_1, \mathbf{l}_2]^T = \begin{pmatrix} s_{11} & s_{12} \\ s_{21} & s_{22} \end{pmatrix} [\mathbf{e}^a, \mathbf{e}^b]^T.$$

Exploiting the fact that  $\hat{\mathbf{T}}^\infty$  is still a stochastic matrix and thus has a constant right Perron eigenvector, we can choose without loss of generality  $\mathbf{1} := \mathbf{r}_1 = (1, \dots, 1)$ . Thus, only one second linear independent right eigenvector  $\mathbf{r}_2$  needs to be computed:

$$(26) \quad \hat{\mathbf{T}}^\infty = [\mathbf{1}, \mathbf{r}_2] \cdot \mathbf{S} \cdot [\mathbf{e}^a, \mathbf{e}^b]^T.$$

Our goal was to compute the committor using (18) which leads us to the following relation for  $\mathbf{q}^A$  and  $\mathbf{q}^B$ , respectively:

$$(27) \quad [\mathbf{q}^A, \mathbf{q}^B] = \hat{\mathbf{T}}^\infty \cdot [\mathbf{e}^a, \mathbf{e}^b]$$

$$(28) \quad = [\mathbf{1}, \mathbf{r}_2] \cdot \mathbf{S}.$$

Thus we have shown that the committor is a linear combination of the right eigenvectors of  $\hat{\mathbf{T}}^\infty$ . To compute the mixing matrix  $\mathbf{S}$  we make use of the fact that the solution of the committor is known already, by definition, in the entries  $a$  and  $b$  for the two states:

$$(29) \quad \begin{pmatrix} q_k^A \\ q_k^B \end{pmatrix} = \begin{pmatrix} \delta_{ak} \\ \delta_{bk} \end{pmatrix} = (\mathbf{1}_k, (\mathbf{r}_2)_k) \cdot \mathbf{S}, \quad k \in \{a, b\}.$$

Writing this as a matrix equation leads to

$$(30) \quad \mathbf{S} = \begin{pmatrix} 1 & (\mathbf{r}_2)_a \\ 1 & (\mathbf{r}_2)_b \end{pmatrix}^{-1},$$

yielding the solutions

$$(31) \quad [\mathbf{q}^A, \mathbf{q}^B] = [\mathbf{1}, \mathbf{r}_2] \cdot \begin{pmatrix} (\mathbf{1})_a & (\mathbf{r}_2)_a \\ (\mathbf{1})_b & (\mathbf{r}_2)_b \end{pmatrix}^{-1},$$

$$(32) \quad q_i = (\mathbf{e}_i \hat{\mathbf{T}}^\infty)_f = \frac{(r_2)_i - (r_2)_a}{(r_2)_b - (r_2)_a}.$$

Finally we have avoided the inversion of the matrix  $\mathbf{R}$  required in (21) and instead reduced the effort to computing one largest nontrivial right eigenvector. This is consistent with the computational effort of solving the system of linear equation in (14).

Based on (32), the committor probability can be easily computed for large sparse transition matrices using, e.g., the Power method [9]. When, instead, the system dynamics are specified in terms of the rate matrix, this computation can be performed by first applying the transformation (15). In the case of the Power method for solving for  $\mathbf{r}_2$ , the parameter  $c$  has to be larger than zero and strictly smaller than 1; otherwise it cannot be proven that all eigenvalues, except one (the Perron eigenvalue  $\lambda_P = 1$ ), are inside the unit circle of the complex plane ( $|\lambda| < 1$ ), assuring convergence to the correct eigenvector. Since in large systems the eigenvalues are expensive to compute, a good guess is to choose  $c$  close to 1, which, in most cases, will maximize the relative gap between the Perron eigenvalues and the next smaller eigenvalues and thus the rate of convergence. The advantages of the Power method are its simplicity, low memory requirement, and applicability to sparse matrices, which allow it to treat very large systems ( $N \sim 10^6$ ) as shown later in the 3D model. However, in the case of slow processes indicated by a very small spectral gap, the Power method might converge too slowly or not at all due to numerical issues. In these cases more advanced methods like Krylov subspace methods (Arnoldi, Lanczos) or graph theoretical approaches [35] can be a solution.

**3.2. Extension to multiple states.** In many applications, it is desirable to compute more than one committor probability. Consider a system for which a number  $M \geq 2$  of core sets have been defined, and for which at each state we wish to evaluate the probability that the system dynamics will hit the core  $i$  rather than any other core. This defines a set of  $M$  committors,  $[\mathbf{q}^{y_1}, \dots, \mathbf{q}^{y_M}]$ , where  $\mathbf{q}^{y_i}$  indicates the vector of committor probabilities of going to core  $i$  next rather than any other core, and each row sums up to 1 ( $\mathbf{q}^{y_1} + \dots + \mathbf{q}^{y_M} = \mathbf{1}$ ), thus forming a membership probability.

To solve this general case, all states  $[Y_1, \dots, Y_M]$  are made absorbing in the transition matrix, and a basis for all eigenvectors of the eigenvalue of 1 is computed. The parameters for the eigenvectors can then be computed using a simple matrix inversion in analogy to the two-state case by

$$(33) \quad [\mathbf{q}^{y_1}, \dots, \mathbf{q}^{y_M}] = [\mathbf{1}, \dots, \mathbf{r}_M] \cdot \begin{pmatrix} \mathbf{1}_{y_1} & \cdots & (\mathbf{r}_M)_{y_1} \\ \vdots & \ddots & \vdots \\ \mathbf{1}_{y_M} & \cdots & (\mathbf{r}_M)_{y_M} \end{pmatrix}^{-1},$$

where  $y_1, \dots, y_M$  are the indices of the states,  $\mathbf{r}_2, \dots, \mathbf{r}_M$  the eigenvectors of the eigenvalue of 1, and  $\mathbf{1}$  is again the constant right Perron eigenvector.

**4. Sensitivity and uncertainty.** We now characterize the sensitivity of the committor  $\mathbf{q}$  to changes in the transition matrix given by  $\frac{\partial q_i}{\partial T_{ab}}$ , and we also examine how the sensitivity leads to a first-order estimate of the uncertainty of the committor  $\delta \mathbf{q}$  in cases where the transition matrix  $\mathbf{T}$  is not exactly known, but is, for example, estimated from simulation data such as from molecular dynamics [27, 28].

**4.1. Sensitivity analysis.** We are interested in  $\frac{\partial \mathbf{q}}{\partial T_{ab}}$ , i.e., the sensitivity of the committor with respect to perturbations in the transition matrix. We define

$\hat{\mathbf{A}} := \hat{\mathbf{T}} - \text{Id}$  so that the null space of  $\hat{\mathbf{A}}$  is the space spanned by the eigenvectors to the eigenvalue of  $\lambda_1 = \lambda_2 = 1$ ; i.e.,

$$(34) \quad \hat{\mathbf{A}}\mathbf{q} = 0.$$

First, we start with the derivative of (34) with respect to  $T_{ab}$ :

$$(35) \quad \frac{\partial \hat{\mathbf{A}}\mathbf{q}}{\partial T_{ab}} = \hat{\mathbf{A}} \cdot \frac{\partial \mathbf{q}}{\partial T_{ab}} + \frac{\partial \hat{\mathbf{A}}}{\partial T_{ab}} \cdot \mathbf{q} = 0.$$

We make the convention that all derivatives are taken at  $T_{ab}$  if not specified otherwise. Since  $\hat{\mathbf{A}}$  does not have full rank and its inverse is not defined, we use

$$(36) \quad \frac{\partial \hat{A}_{ij}}{\partial T_{ab}} = \frac{\partial \hat{T}_{ij}}{\partial T_{ab}} = \begin{cases} \delta_{ia}\delta_{jb}, & i \notin \mathcal{A}, \mathcal{B}, \\ 0, & i \in \mathcal{A}, \mathcal{B}, \end{cases}$$

and then we rewrite this (35) as

$$\sum_k \hat{A}_{ik} \cdot \frac{\partial q_k}{\partial T_{ab}} = -q_b \begin{cases} \delta_{ia}, & i \notin \mathcal{A}, \mathcal{B}, \\ 0, & i \in \mathcal{A}, \mathcal{B}. \end{cases}$$

Since  $\frac{\partial q_k}{\partial T_{ab}} = 0$  for  $k \in \mathcal{A}, \mathcal{B}$ , we can exclude these from the calculation and define a reduced inverse  $\tilde{\mathbf{A}}^{-1}$  given by

$$\tilde{\mathbf{A}}^{-1} = \begin{pmatrix} 0 & \cdots & 0 \\ \vdots & \begin{bmatrix} T_{22} - 1 & \cdots & T_{2,M-1} \\ \vdots & \ddots & \vdots \\ T_{M-1,2} & \cdots & T_{M-1,M-1} - 1 \end{bmatrix}^{-1} & \vdots \\ 0 & \cdots & 0 \end{pmatrix},$$

which is inverted only on the subset of states neither in  $\mathcal{A}$  nor  $\mathcal{B}$ , and the remaining transitions are set to zero, thus assuring the correct boundary conditions for  $\frac{\partial q_i}{\partial T_{ab}}$ . This yields the sensitivity matrix  $S_{ib}^a$  defined by

$$(37) \quad S_{ib}^a := \frac{\partial q_i}{\partial T_{ab}} = - \sum_l \tilde{A}_{il}^{-1} \delta_{la} q_b = -\tilde{A}_{ia}^{-1} q_b.$$

**4.2. Uncertainty and sampling error of the committor.** Let us now consider the case where the transition matrix  $\mathbf{T}$  is not known exactly but is instead sampled by a finite number of observations, as is the case, for example, in molecular dynamics simulations [19, 20, 27, 28]. We will be interested in the question of how the uncertainty involved in this finite sampling translates into uncertainty of the committor. Let  $Z \in \mathbb{R}^{m \times m}$  be a count matrix with  $Z_{ij}$  being the number of independently observed transitions from state  $i$  to state  $j$ . The likelihood of transition matrices pertaining to this observation is given by

$$\mathbb{P}(\mathbf{C} \mid \mathbf{T}) = \prod_{i,j} T_{ij}^{Z_{ij}}.$$

When restricting the prior distribution to the conjugate Dirichlet prior, the posterior distribution can be expressed as

$$\mathbb{P}(\mathbf{T} \mid \mathbf{C}) \propto \mathbb{P}(\mathbf{T})\mathbb{P}(\mathbf{C} \mid \mathbf{T}) = \prod_{i,j} T_{ij}^{B_{ij} + Z_{ij}} = \prod_{i,j} T_{ij}^{C_{ij}},$$

where  $B_{ij}$  are prior counts. Comparing the Dirichlet distribution

$$\prod_i \prod_j T_{ij}^{\alpha_{ij}-1} = \prod_i \text{Dir}(\boldsymbol{\alpha}_i)$$

with  $\boldsymbol{\alpha}_i := \{\alpha_{i1}, \dots, \alpha_{iM}\}$  results in the equivalence

$$(38) \quad \alpha_{ij} = C_{ij} + 1 = B_{ij} + Z_{ij} + 1.$$

The maximum likelihood transition matrix  $\hat{T}_{ij}$  is given by

$$\hat{T}_{ij} = \frac{Z_{ij}}{\sum_k Z_{ik}},$$

the mean of the posterior distributions  $\bar{T}_{ij}$  is given by

$$\bar{T}_{ij} = \frac{\alpha_{ij}}{\sum_k \alpha_{ik}} = \frac{B_{ij} + Z_{ij} + 1}{\sum_k (B_{ik} + Z_{ik} + 1)},$$

and both are equivalent for the null prior  $B_{ij} = -1$ . Equation (38) shows that the prior can be regarded as counts additional to the actual observed counts  $Z_{ij}$ . Thus, to obtain an expectation based mainly on observations, the number of real observations  $Z_{ij}$  must be larger than the number of prior counts:

$$\sum_k Z_{ik} \gg \sum_k (B_{ik} + 1) = m + \sum_k B_{ik}.$$

This forces us to be careful about the choice of the prior, which, in principle, compensates for the lack of information in states with few or none observed transitions.

One choice is the null prior, which sets  $B_{ik} = -1$ , resulting in zero prior counts, and thus the mean and maximum of the posterior probability distribution are equal. Another choice is a uniform prior probability distribution  $\mathbb{P}(T) \propto 1 \Leftrightarrow B_{ij} = 0$ , which will prove inadequate in the cases we consider, since the condition  $\sum_k Z_{ik} \gg m$  is difficult to fulfill when  $m$  is large. A further choice might be to add only a very slight prior to all counts, e.g.,  $B_{ij} = 1 - 1/m$ , and thus request  $\sum_k Z_{ik} \gg 1$ . Yet another approach is to use a prior that has counts restricted to a certain subset of elements. We will address this issue again in the application section.

As we have shown before, the probability distribution can be written as a product of independent Dirichlet distributions for each state. Hence, the covariance between entries in the transition matrix is zero between elements from different rows, and we can define a set of reduced covariance matrices  $\Sigma_{ab}^i$  for each state or equivalently row in the transition matrix  $i$  separately by the expression

$$(39) \quad \Sigma_{ab}^i := \text{Cov}(T_{ia}, T_{ib}) = \frac{\alpha_{ia}(\alpha_i \delta_{ab} - \alpha_{ib})}{\alpha_i^2(\alpha_i + 1)}.$$

This leads finally to an expression for the standard deviation of each entry of the transition matrix:

$$\delta T_{ia} = \sqrt{\text{Cov}(T_{ia}, T_{ia})} = \sqrt{\frac{\alpha_{ia}(\alpha_i - \alpha_{ia})}{\alpha_i^2(\alpha_i + 1)}}$$

with

$$\alpha_i := \sum_{j=1}^m \alpha_{ij}.$$

A simple and often used approach for propagating the uncertainty in  $\mathbf{T}$  to the uncertainty of the committor (or any other property derived from  $\mathbf{T}$ ) is to sample the posterior distribution of transition matrices and compute the committor for each sample of this distribution [19, 28]. However, this procedure involves sampling itself and thus uncertainty in the estimation of the uncertainty, which may be undesirable in situations where the uncertainty estimation is conducted repeatedly, e.g., within an adaptive sampling scheme [27, 28].

An alternative is to propagate the covariance from the transition matrix elements linearly to the covariance in the committor using the computed sensitivity  $S_{ab}^i$  by

$$\begin{aligned} \text{Cov}(q_a, q_d) &= \sum_{i,b,c=1}^m S_{ab}^i \Sigma_{bc}^i (S^T)_{cd}^i \\ &= \sum_{i=1}^m \left( \tilde{\mathbf{A}}^{-1} \right)_{ai} \left( \tilde{\mathbf{A}}^{-1} \right)_{di} \sum_{b,c=1}^m q_b \frac{\alpha_{ib} (\alpha_i \delta_{bc} - \alpha_{ic})}{\alpha_i^2 (\alpha_i + 1)} q_c, \end{aligned}$$

and finally we can compute the variance in the elements of the committor by

$$\begin{aligned} (40) \quad \delta^2 q_a &= \text{Cov}(q_a, q_a) \\ (41) \quad &= \sum_{i=1}^m \frac{1}{\alpha_i^2 (\alpha_i + 1)} \left( \tilde{\mathbf{A}}^{-1} \right)_{ai}^2 \left( \alpha_i \sum_{b=1}^m q_b \alpha_{ib} q_b - \left( \sum_{b=1}^m q_b \alpha_{ib} \right) \left( \sum_{c=1}^m \alpha_{ic} q_c \right) \right). \end{aligned}$$

A complete derivation can be found in the appendix. Clearly, the variance can be separated into contributions from each state  $i$ , and we define an uncertainty contribution vector  $w_i$  by

$$(42) \quad w_i = \sqrt{\sum_{a=1}^m \frac{1}{\alpha_i^2 (\alpha_i + 1)} \left( \tilde{\mathbf{A}}^{-1} \right)_{ai}^2 \left( \alpha_i \sum_{b=1}^m q_b \alpha_{ib} q_b - \left( \sum_{b=1}^m q_b \alpha_{ib} \right) \left( \sum_{c=1}^m \alpha_{ic} q_c \right) \right)},$$

which can then be used in order to direct new simulations that are most promising in reducing the error [27].

## 5. Applications.

**5.1. Diffusion in a 2D three-well potential.** To illustrate an application of the above equations we use a simple model of a particle diffusing in a 2D potential with three wells (Figure 1), partitioned into a grid of  $m = 30 \cdot 30 = 900$ . The minima and their associated regions of configurational space will be referred to as  $A$ ,  $B$ , and  $C$ . Transition probabilities are defined based on the potential energies  $U_i$  on each grid point using a Metropolis acceptance criterion given by

$$(43) \quad T_{ij} = \frac{\mathbb{P}(i \rightarrow j)}{\sum_k \mathbb{P}(i \rightarrow k)} = \frac{\min(1, \exp(-\beta(U_j - U_i)))}{\sum_k \min(1, \exp(-\beta(U_k - U_i)))}$$

with  $\beta = 1$ , which has the correct invariant distribution  $\pi_i \propto \exp(-\beta U_i)$ . Only transitions between horizontal or vertical neighboring microstates are allowed, resulting in a maximum of five nonzero entries per row in the 900x900 transition matrix. This matrix is used as the reference for the dynamics of the system. The committor from state  $A$  to  $B$ , as given in (32), is shown in Figure 2.

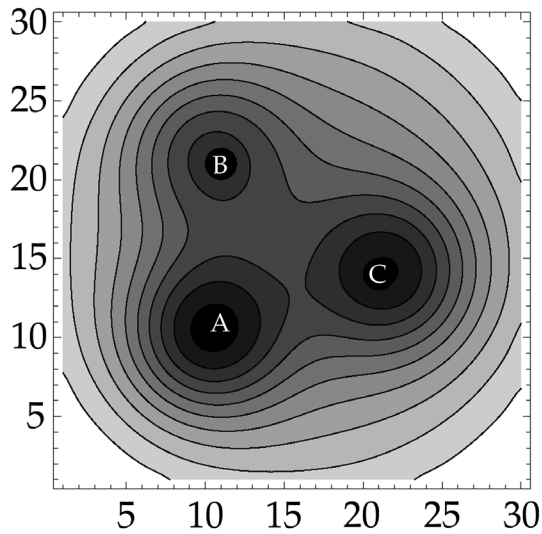


FIG. 1. Energy landscape for diffusion in a 2D potential with three basins discretized into a grid of  $30 \times 30$  bins. The minima in each basin are indicated by the letters A, B, and C. Black indicates low energies; white, high energies.

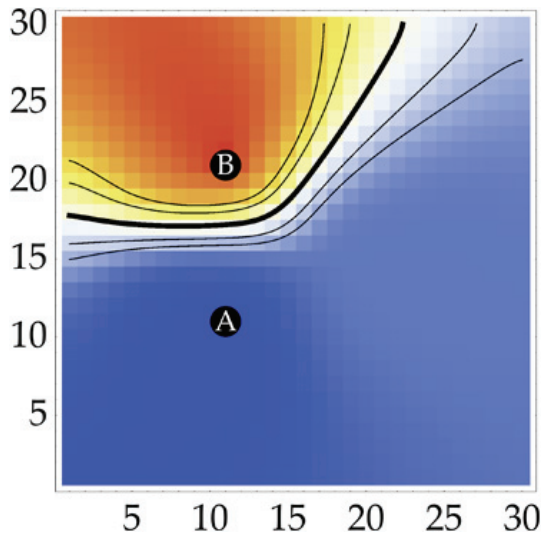


FIG. 2. 2D three-well model: committor from state A to C computed directly from the reference transition probability matrix  $T_{ij}$ .

To investigate the dependence of the committor and its uncertainty on the actual number of observations and the chosen prior probability distribution, we computed the expected number of observed transitions in an equilibrium simulation as

$$\bar{Z}_{ij} = L \pi_i \hat{T}_{ij},$$

which is the product of the total number of simulation steps  $L$ , the invariant density of a state  $\pi_i$ , and the true transition probabilities  $\hat{T}_{ij}$ . Four different types of prior distributions are considered here (see Table 1). The committors computed for different

TABLE 1  
*Prior probability distributions used for the 2D example.*

Prior	$B_{ij}$
Null Prior	-1
1/m Prior	$1/m - 1$
Neighbor Prior	$\begin{cases} 0 & \text{if } (i, j) \text{ neighbors} \\ -1 & \text{else} \end{cases}$
Uniform Prior	0

simulation lengths  $L = \{10^1, 10^3, 10^5, 10^7\}$  and all prior sets except the null prior are presented in Figure 3. The null prior was omitted since in this case the committor does not depend on the simulation length  $L$  and equals the exact committor (Figure 2). It is important to note that this equivalence is only true on average and not for every possible simulation outcome. The influence of the full uniform prior is so strong that the computed committor differs from the true committor vastly even for  $L = 10^7$ . The other two priors behave similarly to each other while the neighbor prior has the general advantage over the null prior that it always provides a transition matrix that can numerically be evaluated.

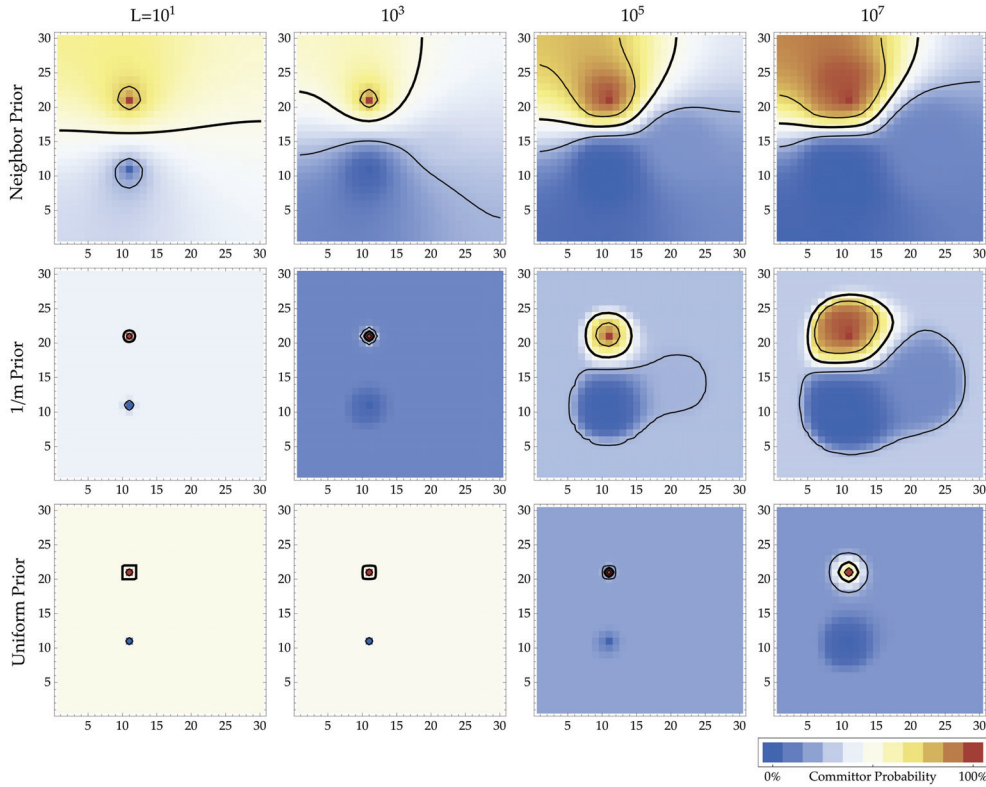


FIG. 3. 2D three-well model: committor from state A to C computed for different prior choices (rows: neighbor prior, 1/m prior, full uniform) and simulation lengths (columns:  $L = \{10^1, 10^3, 10^5, 10^7\}$ ). Isocommittor surfaces for  $q = \{0.25, 0.5, 0.75\}$  are given in black.

Equation (40) gives the expression for the uncertainty in the computed average committor from a given number of observations. For the same set of total observations  $L$  and all priors in Table 1 the covariance was computed and is shown in Figure 4. The main uncertainty is always greatest in the transition region, and it depends strongly on the choice of the prior, especially when few observations have been made.

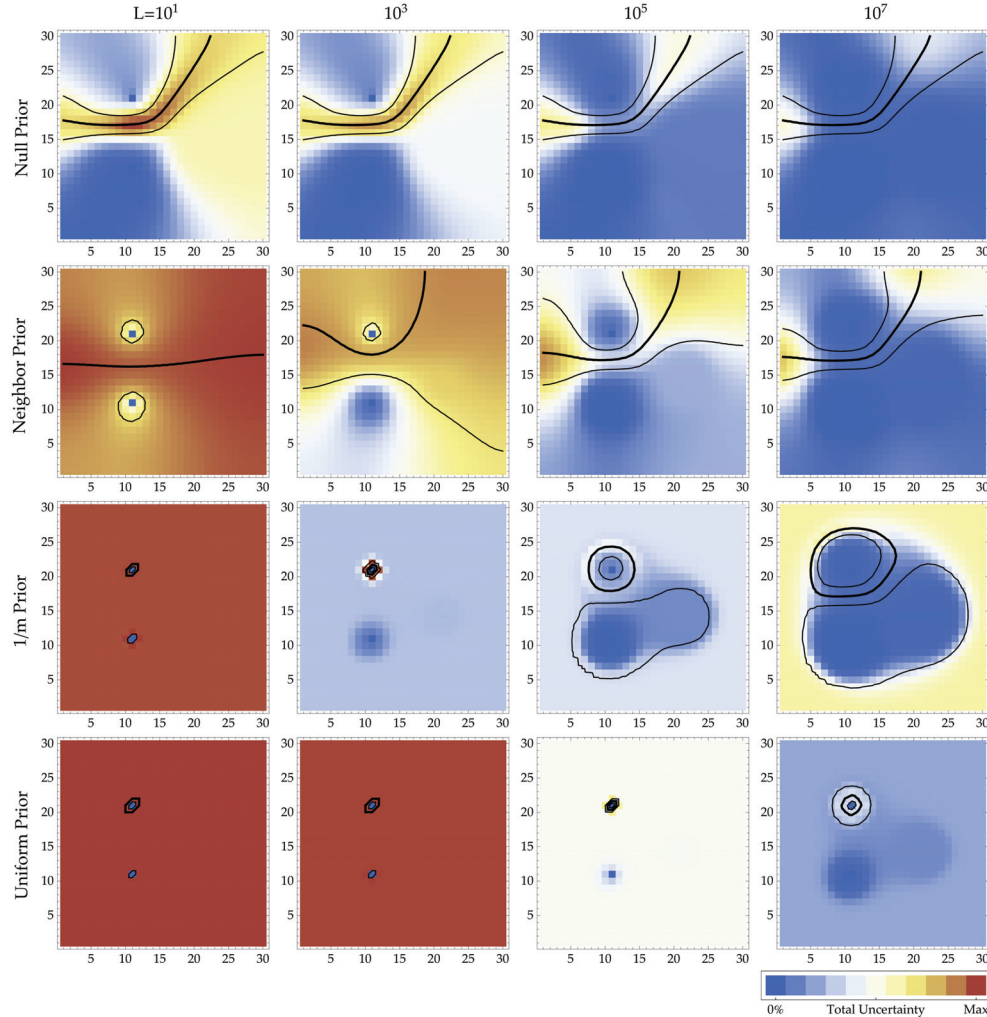


FIG. 4. 2D three-well model: statistical uncertainty (variance) in the entries of the committor probability  $\text{Cov}(q_i, q_i)$  in (40) from state A to B for different prior choices (rows: null prior, neighbor prior,  $1/m$  prior, full uniform) and simulation lengths (columns:  $L = \{10^1, 10^3, 10^5, 10^7\}$ ). Isocommittor surfaces from Figure 3 shown in black. Blue indicates no variance; red indicates high variance. The related absolute error development is given in Figure 6. States A and B are fixed by definition, thus at these points the variance is equal to zero. The highest variation is found in the transition region, the size of which depends strongly on the prior information. With increasing simulation length, the error in the low energy states reduces fastest.

Figure 5 shows the difference in the predicted committors compared to the true reference committor given in Figure 2. The quality of the average predicted committor depends mainly on the amount of prior information put into the predictions: Priors

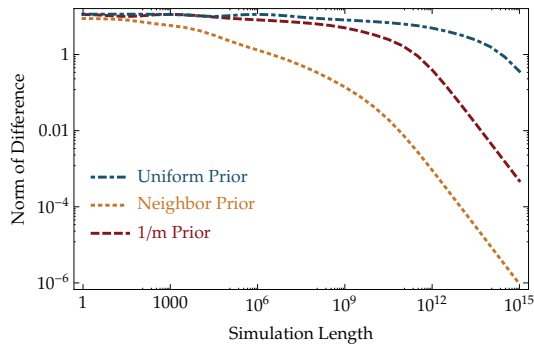


FIG. 5. 2D three-well model: norm of the difference of the computed committor for different prior probability distributions (neighbor prior,  $1/m$  prior, full uniform) versus simulation length  $L$ . The uniform estimation is about six orders of magnitude slower in convergence since the amount of prior information is also about six orders of magnitude larger compared to the other priors.

with little information (null prior, neighbor prior) have less bias, while priors with much information ( $1/m$  prior, uniform prior) strongly bias the computed committor. However, committors with much information are less sensitive to perturbations in the transition matrix elements (see Figure 6), thus having smaller uncertainties. However, due to the bias, this uncertainty is misleading in the cases of few observations. This behavior changes once the simulation length is long enough for the estimated committors to be similar.

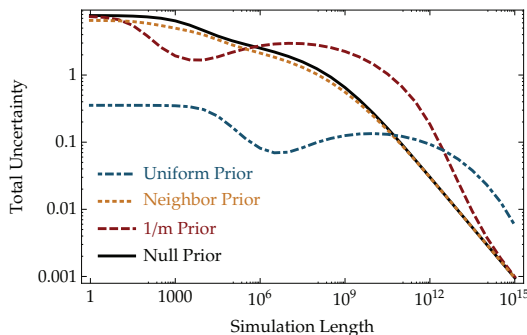


FIG. 6. 2D three-well model: theoretical average uncertainty in the estimated committor for different prior probability distributions (null prior, neighbor prior,  $1/m$  prior, full uniform) versus simulation length  $L$ . The initial erratic behavior of the  $1/m$  prior and uniform prior is caused by a wrong committor prediction due to the high impact of these priors when only few transitions have been observed.

The effects of the bias of the prior are also visible in the contribution to the uncertainty from each state  $i$  given by  $w_i$  in (42) as shown in Figure 7. In general, the main contributions to the uncertainty are located in states inside the transition region. For small simulation lengths  $L$  the contribution is more widely distributed and mainly in regions that have also a significant equilibrium probability. With increasing simulation time, the uncertainty contributing states shift toward the outer perimeter of the energy landscape, where the uncertainty remains mostly unchanged since these parts of phase space are hardly visited at all. The net flux for the system as given

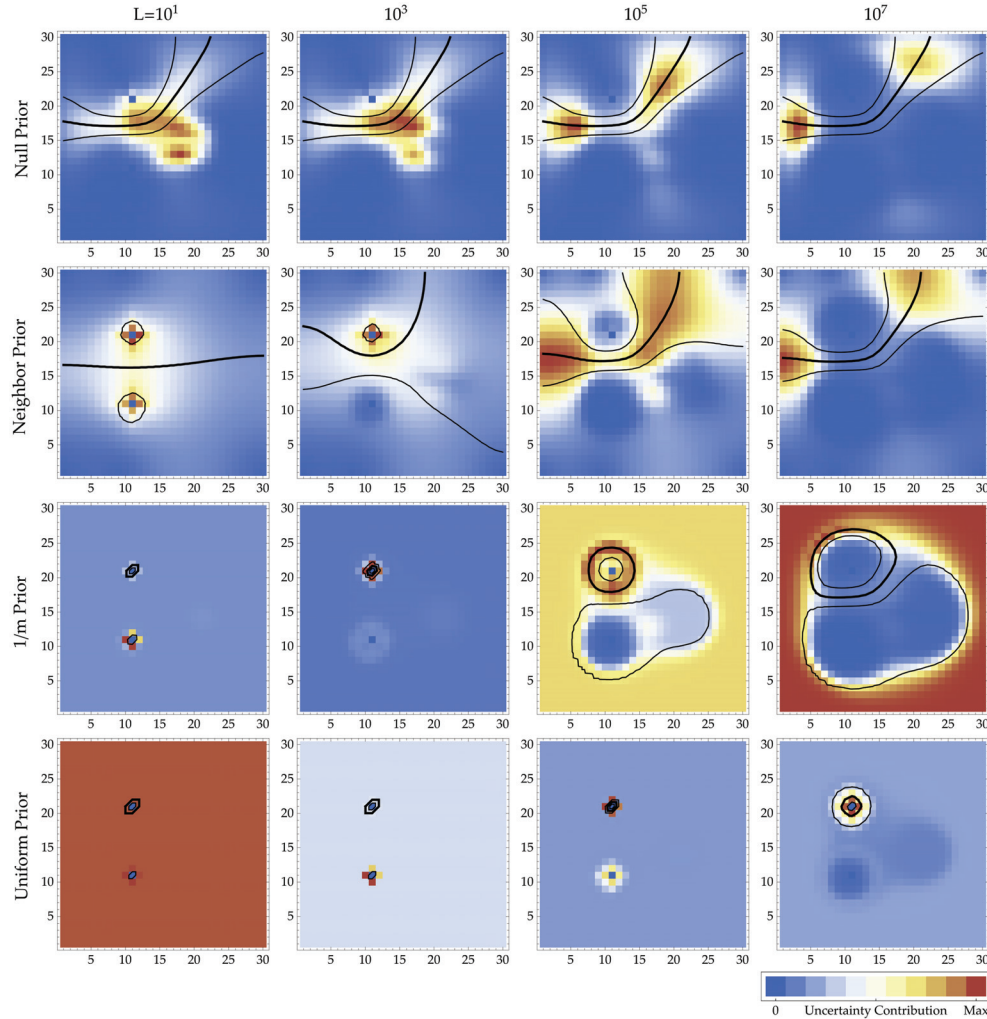


FIG. 7. 2D three-well model: Uncertainty contribution vector  $w_i$  in (42) for different prior choices (rows: null prior, neighbor prior,  $1/m$  prior, full uniform) and simulation lengths (columns:  $L = \{10^1, 10^3, 10^5, 10^7\}$ ). Isocommittor surfaces from Figure 3 shown in black. Blue indicates vanishing sensitivity, red maximal sensitivity for each plot separately, thus absolute comparison is not possible between plots. This was chosen to better indicate the highest uncertainty contributions. The absolute sensitivity is given in Figure 6. The figure shows that in the case of the uniform prior a length of  $L = 10^7$  is insufficient for an accurate description of the uncertainty.

by (8) is shown in Figure 8. The opacity of the arrows indicates the intensity of the flux in the direction of the arrow. The main fraction of the flux traverses the barrier between  $A$  and  $B$ , while a minor fraction travels over state  $C$ . Finally, the three-state committor, given by (33), was computed for states  $A$ ,  $B$ , and  $C$  (see Figure 9), thus partitioning the configurational space into three subsets divided by the main barriers. In this manner the multistate committor can be used to partition the configurational space into subsets that are dynamically close to one state of a set of predefined states which can be regarded as cluster centers.

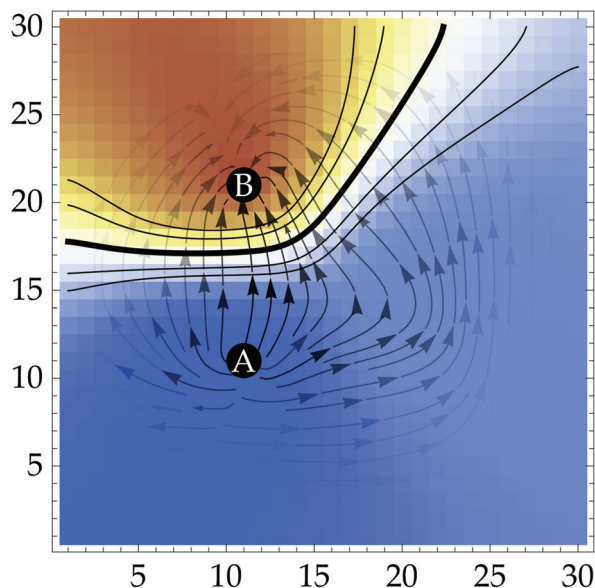


FIG. 8. 2D three-well model: net flux between states A and B computed from the reference transition matrix  $\hat{T}_{ij}$ . The underlying colors represent the reference committor. Arrows indicate the direction of the flux and the opacity the intensity. Most flux travels over the direct barrier from state A to state B.

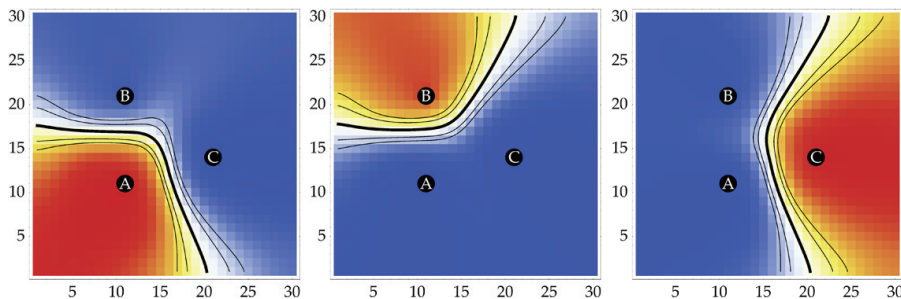


FIG. 9. Committor computed for three states from (33). The committor shows a clear separation of the configurational space into three subsets divided by the potential barriers.

**6. 3D model.** The method is now further examined on a simple model system that mimics diffusional protein-ligand association. For this, a 3D potential was defined by a potential function  $U$ :

$$U(x) = \sum_{i=1}^5 \frac{b_i}{\sqrt{2\pi\sigma^2}} \exp\left(-\frac{(x - \bar{x}_i)^2}{2\sigma_i^2}\right).$$

This sum of five 3D Gaussian functions mimics an electrical field in which the ligand diffuses (for parameters see Table 2).

The potential was coarse-grained on a grid with a total of  $m = 100 \cdot 100 \cdot 100 = 10^6$  states in the range of  $[-1, 1]^3$ . The dynamics were modeled as a diffusional process under the influence of the potential as in the previous 2D case (see (43)). Figure 10 shows equipotential surfaces for a set of 19 exponentially spaced values of the potential  $U$ , effectively depicting surfaces of equal equilibrium probability.

TABLE 2  
 3D protein-ligand model: parameters for the manually defined potential  $U$ .

$i$	Sign $b_i$	Mean $\bar{x}$	Std Dev $\sigma$
1	-	{0.0, 0.0, -0.2}	0.10
2	-	{-0.6, 0.2, -0.6}	0.08
3	-	{-0.6, 0.4, 0.4}	0.08
4	+	{0.4, -0.6, -0.6}	0.05
5	-	{-0.6, -0.6, -0.6}	0.05

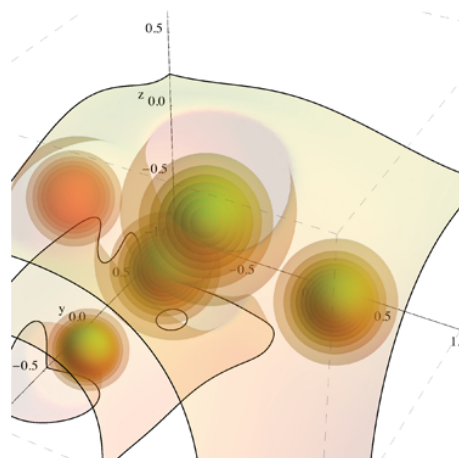


FIG. 10. 3D protein-ligand model: equipotential surfaces.

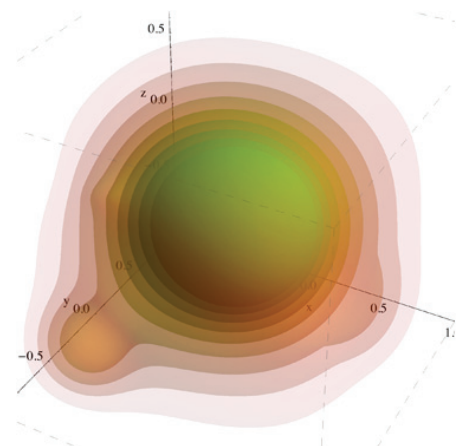


FIG. 11. 3D protein-ligand model: isocommittor surfaces for the potential  $U$ .

The outer boundary of the grid is defined as the “unbound” state  $\mathcal{A}$ , while all states inside a sphere at the center of the grid with a radius of 0.2 define the “bound” state  $\mathcal{B}$ . The committor probability was computed using the procedure described in the theory section, employing the Power method to solve for the dominant eigenvector of the absorbing process [9]. The isocontours of the committor are shown in Figure 11. It is seen that these contours are roughly spherical around the binding site  $B$  but have protrusions due to the existence of local energy minima.

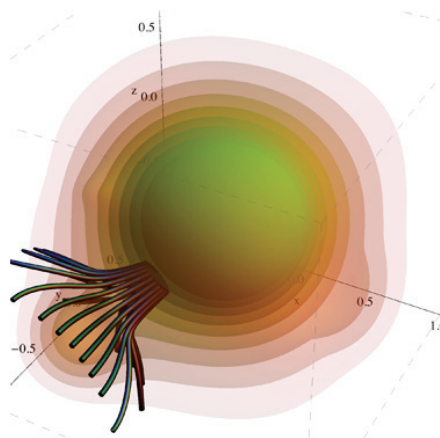


FIG. 12. 3D protein-ligand model: bundle of path lines starting at the virtual binding site along the normals to the isocommittor surfaces.

Figure 12 shows some paths integrated along the normals to the isocommittor hypersurfaces. To compute these, the committor function, given on each grid point, was interpolated by linear polynomials between each neighboring grid point, and the normals were computed from the continuous interpolation. As initial points, 20 circularly positioned points on the inner  $\mathcal{B}$  state were chosen, which were directed toward the potential minimum at point 5 in Table 2. The integrated paths define a bundle of field lines connecting the outer perimeter and the binding site, depicting the most probable paths toward the virtual binding site on the protein.

Using the committor, the reactivity  $g$  [17], i.e., the probability that a state contributes to a reactive trajectory, was also computed, using

$$(44) \quad g_i = q_i^+ \pi_i q_i^-.$$

The results are shown in Figure 13. Due to the higher equilibrium probability in (44), the density of reactive trajectories increases toward the binding site and especially in the local minima.

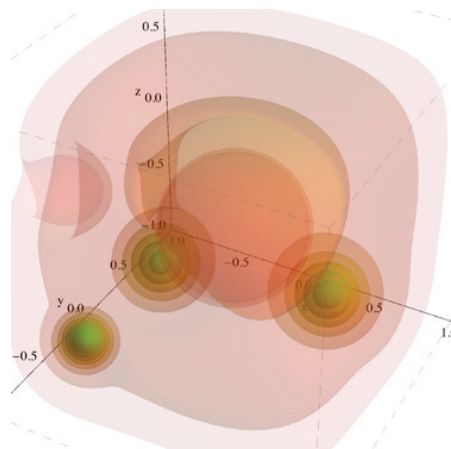


FIG. 13. 3D protein-ligand model: density of reactive trajectories  $g_i$  as given in (44).

**7. Conclusions.** We have conducted a numerical study of the committor probability—the central mathematical object for characterizing dynamical processes—for discrete-state Markov processes.

An eigenvector-based approach to compute the committor probability was derived. This method is efficient, easy to implement, and computes the committor for dynamical systems with large state spaces. If the considered transition matrix is sparse enough, even very large systems can be investigated with computational effort roughly proportional to the number of states, and thus the application of the presented method is limited only by memory constraints. As an example, it was demonstrated that the approach is able to investigate the electrostatically steered ligand binding pathways to a protein.

Furthermore, a sensitivity and error analysis of the committor was conducted. Computation of the sensitivity requires the inversion of a matrix of the size of the number of states, which is, in general, of cubic order, but it can be made quadratic if the matrix is sufficiently sparse. The other computations are also maximally of quadratic order, which, in principle, also allows a sensitivity analysis for medium system sizes.

The obtained error analysis allows an adaptive algorithm to be defined for fast computation of the committor by collecting information from different parts of the configurational space separately. This can produce more accurate estimations than possible from one single long simulation.

### Appendix.

**Proof of Theorem 1.** For arbitrary  $\mathcal{A}$  and  $\mathcal{B}$ , we need to show that if  $\mathbf{K}$  fulfills the committor equations for rate matrices, then  $\mathbf{T}(\mathbf{K})$  has to fulfill the committor equation for transition matrices. By definition this is true for all states  $x \in \mathcal{A} \cup \mathcal{B}$ . For all other states we start with the committor equation for transition matrices and replace the transition matrix by  $\mathbf{T}(\mathbf{K})$  and get

$$\sum_{j \in I} (c \cdot K_{ij} + \delta_{ij}) q_j^+ = q_i^+,$$

which can be simplified to the committor equation for rate matrices:

$$c \cdot \sum_{j \in I} K_{ij} q_j^+ = 0.$$

The theorem is independent of the choice of  $c$ , but  $0 < c < c_{max}$  assures that the row sum of zero in the rate matrix translates into row-stochastic transition matrix  $\mathbf{T}(\mathbf{K})$ . A more direct proof is the fact that scaling of matrices by a constant factor and adding multiples of the identity matrix do not change the eigenvectors of a matrix. Thus  $\mathbf{T}(\mathbf{K})$  inherits the same eigenvectors as  $\mathbf{K}$ , but with different eigenvalues. Since we show that, aside from the boundary conditions, the committor can be computed from the eigenvectors, both matrices will result in the same committor probabilities. However, it is important to note that  $\mathbf{T}(\mathbf{K})$  will not reproduce the dynamical behavior of the rate matrix  $\mathbf{K}$  on any but infinite timescales.

**Derivation of the committor covariance.** To derive the committor covariance, we start with the linear error propagation for the committor and use the sensitivity  $\mathbf{S}$ , given in (37), to extend the error in the transition matrix  $\sum$  as follows:

$$\begin{aligned}
 \text{Cov}(q_a, q_d) &= \sum_{i,b,c=1}^m S_{ab}^i \Sigma_{bc}^i (S^T)^i_{cd} \\
 &= \sum_{i,b,c=1}^m \frac{\partial \tilde{q}_a}{\partial T_{ib}} \Sigma_{bc}^i \frac{\partial \tilde{q}_d}{\partial T_{ic}} \\
 &= \sum_{i,b,c=1}^m \left( \tilde{\mathbf{A}}^{-1} \right)_{ai} q_b \Sigma_{bc}^i \left( \tilde{\mathbf{A}}^{-1} \right)_{di} q_c \\
 &= \sum_{i=1}^m \left( \tilde{\mathbf{A}}^{-1} \right)_{ai} \left( \tilde{\mathbf{A}}^{-1} \right)_{di} \sum_{b,c=1}^m q_b \Sigma_{bc}^i q_c.
 \end{aligned}$$

We then insert the analytical expression for the uncertainty in the transition matrix in (39) to obtain

$$\text{Cov}(q_a, q_a) = \sum_{i=1}^m \left( \tilde{\mathbf{A}}^{-1} \right)_{ai} \left( \tilde{\mathbf{A}}^{-1} \right)_{di} \sum_{b,c=1}^m q_b \frac{\alpha_{ib} (\alpha_i \delta_{bc} - \alpha_{ic})}{\alpha_i^2 (\alpha_i + 1)} q_c.$$

This can be rewritten in a form that is quadratic in the number of states:

$$\text{Cov}(q_a, q_a) = \sum_{i=1}^m \frac{1}{\alpha_i^2 (\alpha_i + 1)} \left( \tilde{\mathbf{A}}^{-1} \right)_{ai}^2 \left( \alpha_i \sum_{b=1}^m q_b \alpha_{ib} q_b - \left( \sum_{b=1}^m q_b \alpha_{ib} \right) \left( \sum_{c=1}^m \alpha_{ic} q_c \right) \right),$$

leaving us with the inversion of  $\tilde{\mathbf{A}}$  as the most expensive operation of cubic order.

#### REFERENCES

- [1] A. M. BEREZHKOVSII AND A. SZABO, *Ensemble of transition states for two-state protein folding from the eigenvectors of rate matrices*, J. Chem. Phys., 121 (2004), pp. 9186–9187.
- [2] R. B. BEST AND G. HUMMER, *Reaction coordinates and rates from transition paths*, Proc. Natl. Acad. Sci. USA, 102 (2005), pp. 6732–6737.
- [3] P. G. BOLHUIS, D. CHANDLER, C. DELLAGO, AND P. L. GEISSLER, *Transition path sampling: Throwing ropes over rough mountain passes, in the dark*, Annu. Rev. Phys. Chem., 53 (2002), pp. 291–318.
- [4] N.-V. BUCHETE AND G. HUMMER, *Peptide folding kinetics from replica exchange molecular dynamics*, Phys. Rev. E, 77 (2008), 030902.
- [5] C. DELLAGO, P. G. BOLHUIS, AND P. L. GEISSLER, *Transition path sampling*, Adv. Chem. Phys., 123 (2002), pp. 1–84.
- [6] R. DU, V. S. PANDE, A. Y. GROSBERG, T. TANAKA, AND E. I. SHAKHNOVICH, *On the transition coordinate for protein folding*, J. Chem. Phys., 108 (1998), pp. 334–350.
- [7] WEINAN E, W. REN, AND E. VANDEN-EIJNDEN, *Transition pathways in complex systems: Reaction coordinates, isocommittor surfaces, and transition tubes*, Chem. Phys. Lett., 413 (2005), pp. 242–247.
- [8] B. ENSING, A. LAIO, F. L. GERVASIO, M. PARRINELLO, AND M. L. KLEIN, *A minimum free energy reaction path for the e2 reaction between fluoro ethane and a fluoride ion*, J. Amer. Chem. Soc., 126 (2004), pp. 9492–9493.
- [9] G. H. GOLUB AND C. F. VAN LOAN, *Matrix Computation*, 3rd ed., Johns Hopkins University Press, Baltimore, MD, 1996.
- [10] I. HORENKO, *Finite element approach to clustering of multidimensional time series*, SIAM J. Sci. Comput., 32 (2010), pp 62–83.
- [11] I. HORENKO, R. KLEIN, S. DOLAPTCHIEV, AND C. SCHÜTTE, *Automated generation of reduced stochastic weather models. I: Simultaneous dimension and ...*, Multiscale Model. Simul., 6 (2008), pp. 1125–1145.
- [12] G. HUMMER, *From transition paths to transition states and rate coefficients*, J. Chem. Phys., 120 (2004), pp. 516–523.

- [13] P. LENZ, B. ZAGROVIC, J. SHAPIRO, AND V. S. PANDE, *Folding probabilities: A novel approach to folding transitions and the two-dimensional Ising-model*, J. Chem. Phys., 120 (2004), pp. 6769–6778.
- [14] A. MA AND A. R. DINNER, *Automatic method for identifying reaction coordinates in complex systems*, J. Phys. Chem. B, 109 (2005), pp. 6769–6779.
- [15] L. MARAGLIANO, A. FISCHER, E. VANDEN-EIJNDEN, AND G. CICCOTTI, *String method in collective variables: Minimum free energy paths and isocommittor surfaces*, J. Chem. Phys., 125 (2006), 24106.
- [16] P. METZNER, E. DITTMER, T. JAHNKE, AND C. SCHÜTTE, *Generator estimation for Markov jump processes*, J. Comput. Phys., 227 (2007), pp. 353–375.
- [17] P. METZNER, C. SCHÜTTE, AND E. VANDEN-EIJNDEN, *Transition path theory for Markov jump processes*, Multiscale Model. Simul., 7 (2009), pp. 1192–1219.
- [18] H. MORI, *Transport, collective motion, and Brownian motion*, Progr. Theoret. Phys., 33 (1965), pp. 423–455.
- [19] F. NOÉ, *Probability distributions of molecular observables computed from Markov models*, J. Chem. Phys., 128 (2008), 244103.
- [20] F. NOÉ AND S. FISCHER, *Transition networks for modeling the kinetics of conformational change in macromolecules*, Curr. Opin. Struct. Biol., 18 (2008), pp. 154–162.
- [21] F. NOÉ, C. SCHÜTTE, E. VANDEN-EIJNDEN, L. REICH, AND T. R. WEIKL, *Constructing the equilibrium ensemble of folding pathways from short off-equilibrium simulations*, Proc. Natl. Acad. Sci. USA, 106 (2009), 19011–6.
- [22] J. R. NORRIS, *Markov Chains*, Cambridge University Press, New York, 1998.
- [23] A. C. PAN AND D. CHANDLER, *Dynamics of nucleation in the Ising model*, J. Phys. Chem. B, 108 (2004), pp. 19681–19686.
- [24] V. S. PANDE, A. Y. GROSBERG, T. TANAKA, AND D. S. ROKHSAR, *Pathways for protein folding: Is a new view needed?*, Curr. Opin. Struct. Biol., 8(1) (Feb 1998), pp. 68–79.
- [25] B. PETERS AND B. L. TROUT, *Obtaining reaction coordinates by likelihood maximization*, J. Chem. Phys., 125 (2006), 054108.
- [26] M. SARICH, F. NOÉ, AND C. SCHÜTTE, *On the approximation quality of Markov state models*, Multiscale Model. Simul., 8 (2010), pp. 1154–1177.
- [27] N. SINGHAL AND V. S. PANDE, *Error analysis and efficient sampling in Markovian state models for molecular dynamics*, J. Chem. Phys., 123 (2005), 204909.
- [28] N. SINGHAL, C. D. SNOW, AND V. S. PANDE, *Using path sampling to build better Markovian state models: Predicting the folding rate and mechanism of a tryptophan zipper beta hair-pin*, J. Chem. Phys., 121 (2004), pp. 415–425.
- [29] A. SPAAR, C. DAMMER, R. R. GABDOULLINE, R. C. WADE, AND V. HELMS, *Diffusional encounter of barnase and barstar*, Biophys. J., 90 (2006), pp. 1913–1924.
- [30] P. J. STEINHARDT, D. R. NELSON, AND M. RONCHETTI, *Bond-orientational order in liquids and glasses*, Phys. Rev. B, 28 (1983), pp. 784–805.
- [31] F. TAKENS, *Detecting strange attractors in turbulence*, in Dynamical Systems and Turbulence, Volume 898, D.A. Rand and L.-S. Young, eds., Springer, New York, 1981, pp. 366–381.
- [32] H. TAKETOMI, Y. UEDA, AND N. GO, *Studies on protein folding, unfolding and fluctuations by computer simulation. I. The effect of specific amino acid sequence represented by specific inter-unit interactions*, Int. J. Pept. Prot. Res., 7 (1975), pp. 445–459.
- [33] E. VANDEN-EIJNDEN, *Transition path theory*, in Computer Simulations in Condensed Matter Systems: From Materials to Chemical Biology, Volume 1, M. Ferrari, G. Ciccotti, and K. Binder, eds., Springer, New York, 2006, pp. 453–493.
- [34] D. J. WALES, *Energy landscapes: Calculating pathways and rates*, Int. Rev. Phys. Chem., 25 (2006), pp. 237–282.
- [35] D. J. WALES, *Calculating rate constants and committor probabilities for transition networks by graph transformation*, J. Chem. Phys., 130 (2009), 204111.
- [36] R. W. ZWANZIG, *Memory effects in irreversible thermodynamics*, Phys. Rev., 124 (1961), pp. 983–992.
- [37] R. W. ZWANZIG, *Nonequilibrium Statistical Mechanics*, Oxford University Press, London, 2001.